remote sensing

MDPI

Article

Study on the Pretreatment of Soil Hyperspectral and Na^+ Ion Data under Different Degrees of Human Activity Stress by Fractional-Order Derivatives

Anhong Tian [1,2], Junsan Zhao [2,*], Bohui Tang [2], Daming Zhu [2], Chengbiao Fu [1,2] and Heigang Xiong [3,4]

1 College of Information Engineering, Qujing Normal University, Qujing 655011, China; tianah@mail.qjnu.edu.cn (A.T.); fucb@mail.qjnu.edu.cn (C.F.)
2 Faculty of Land Resource Engineering, Kunming University of Science and Technology, Kunming 650093, China; tangbh@kust.edu.cn (B.T.); 11301066@kust.edu.cn (D.Z.)
3 College of Applied Arts and Science, Beijing Union University, Beijing 100083, China; heigang@buu.edu.cn
4 College of Resource and Environment Sciences, Xinjiang University, Urumqi 830046, China
* Correspondence: jszht@kmust.edu.cn; Tel.: +13-70-8441-869

Abstract: Soluble salts in saline soil often exist in the form of salt base ions, and excessive water-soluble base ions can harm plant growth. As one of the water-soluble base ions, Na+ ion, is the main indicator of the degree of soil salinization. The pretreatment of visible, near infrared and short-wave infrared (VNIR-SWIR) spectroscopy data is the key to establishing a high-precision inversion model, and a proper pretreatment method can fully extract the effective information hidden in the hyperspectral data. Meanwhile, different degrees of human activity stress will have an impact on the ecological environment of oases. However, there are few comparative analyses of the data pretreatment effects for soil water-soluble base ions on the environment under different human interference conditions. Therefore, in this study, the difference in the degree of soil disturbance caused by human activities was used as the basis for dividing the experimental area into lightly disturbed area (Area A), moderately disturbed area (Area B) and severely disturbed zone (Area C). The Grünwald-Letnikov fractional-order derivative (FOD) was used to preprocess the VNIR-SWIR spectroscopic data measured by a FieldSpec®3Hi-Res spectrometer, which could fully extract the useful information hidden in the FOD of the VNIR-SWIR spectroscopy results and avoid the loss of information caused by the traditional integer-order derivative (1.0-order, 2.0-order) pretreatment. The spectrum pretreatment was composed of five transform spectra (R, $\sqrt{R}$, 1/R, lgR, 1/lgR) and 21 FOD methods (step size is 0.1, derivative range is from 0.0- to 2.0-order). In addition, this manuscript compares and analyzes the pretreatment advantages between fractional-order and integer-order. The main results were as follows: (1) Grünwald-Letnikov FOD can reveal the nonlinear characteristics and variation laws of the field hyperspectral of saline soil, namely, due to the continuous performance of the order selection, the FOD accurately depicts the details of spectral changes during the derivation process, and improves the resolution between the peaks of the hyperspectral spectrum. (2) There is a big difference in the shape of the correlation coefficient curve between the original hyperspectral and Na+ at different FOD. The correlation coefficient curve has a clear outline in rang of the 0.0- to 0.6-order, and the change trend is gentle, which presents a certain gradual form. With the continuous increase of the order of the FOD, the change range of the correlation coefficient curve is gradually increased, and the fluctuation is greater between the 1.0-order and the 2.0-order. (3) Regardless of the transformation spectrum and different interference regions, the improvement effect of the FOD on the correlation between hyperspectral and Na+ is significantly better than that of the integer-order derivative. Comparative analysis shows that he percentage of increase of the former is more than 3%, and the highest is more than 17%.

Keywords: Grünwald-Letnikov fractional-order derivative (FOD); hyperspectral resolution; correlation; different degrees of human activity stress; pretreatment

Citation: Tian, A.; Zhao, J.; Tang, B.; Zhu, D.; Fu, C.; Xiong, H. Study on the Pretreatment of Soil Hyperspectral and Na^+ Ion Data under Different Degrees of Human Activity Stress by Fractional-Order Derivatives. *Remote Sens.* **2021**, *13*, 3974. https://doi.org/10.3390/rs13193974

Academic Editor: Eyal Ben-Dor

Received: 7 August 2021
Accepted: 30 September 2021
Published: 4 October 2021

1. Introduction

Soil is an important natural resource that is vital to the survival of life on Earth. The salt level is an important attribute of soil [1]. A proper salt content can provide the ions needed for the growth and development of plants, while a higher salt content will cause "salt damage" to the growth of plants, such as salt stress, salt-alkali stress and alkali stress. Therefore, the salt information obtained quickly and accurately is the key to the improvement of saline soil, for example, Metternicht et al. [2] introduced the potentials and constraints of remote sensing of soil salinity. The soil salinity caused by natural or human-induced processes is considered a major environmental hazard, and the paper reviewed various sensors and approaches used for remote identification and mapping of salt-affected areas, in order to curb degradation trends and secure sustainable land use. Farifteh et al. [3] predicted the salt concentrations in soils using partial least squares regression (PLSR) and an artificial neural network (ANN). Their results showed that either of the two methods was satisfactory for establishing the relationship between soil electrical conductivity (EC) and soil reflectance, which indicates that the relation between soil salinity and soil reflectance could be approximated by a linear function. Peng et al. [4] estimated soil salinity in Xinjiang using a PLSR model and a cubist model, and the results indicated that cubist model could predict EC values with better accuracy and stability under variable environmental conditions than PLSR, and the cubist model was recommended for mapping soil salinity under environmental conditions with a large spatial variation of vegetation, soil moisture and salinization.

Most of the saline soils in Xinjiang mainly contain water-soluble chlorides and sulfates, and the soluble salts in saline soils often exist in the form of base ions (which refers to the CO_3^{2-}, Cl^-, SO_4^{2-}, Na^+, Ca^{2+}, Mg^{2+} ions generated after the dissociation of sodium salts, magnesium salts and calcium salts). The characteristics of water-soluble base ions can show the migration trend of total salt to a certain extent. They are an important factor in the response of soil hyperspectral reflectivity and can be used as a characteristic factor of soil salinization. As one of the water-soluble base ions, Na+ ion is the main indicator of the degree of soil salinization [5], and the accurate estimation of its content can provide important technical support for the treatment of saline soils.

The traditional method of obtaining salt content information content is to collect a limited number of soil samples in the field, and then bring the samples back to the laboratory for chemical analysis. Although the salt information content information provided by this method has high accuracy, it has the disadvantages of expensive labor costs, long test cycles, low real-time efficiency and being time-consuming and laborious, which cannot meet the demands of dynamic, rapid, accurate monitoring and evaluation of saline soils from a large-scale perspective. However, hyperspectral remote sensing technology has the advantages of being dynamic, fast, accurate, pollution-free, non-destructive, with wide coverage, high resolution, and multiple bands [6], and it has become a convenient and efficient method to monitor soil salinization. For example, Wang et al. [7] collected soil samples from the Hetao area in Inner Mongolia. Three methods of gray correlation, stepwise regression and variable importance projection (VIP) were used to screen the characteristic bands of the eight major ions. The paper studied the inversion performance of PLSR and support vector machine (SVM) models for ions. It is found that the model established by the spectra data pretreated by VIP has the best accuracy, the prediction effect of PLSR is better than that of SVM, and the model can better predict Na^+, Mg^{2+}, Ca^{2+}, SO_4^{2-} and Cl^- ions, while the prediction performance of K^+, CO_3^{2-} and HCO_3^- ions is poor. Srivastava et al. [8] collected soil samples from farmers' fields in three villages in the Ganges Plain, India, and used the PLSR model to predict soil salinity information. Their simulation showed that the 1390–2400 nm band can successfully predict the saline soil information. It has strong predictive ability for electrical conductivity, Na^+, and Cl^-, as well as good predictive ability for Ca^{2+}, good predictive ability for SO_4^{2-}, and poor predictive ability for CO_3^{2-}, PH, and HCO_3^-.

The pretreatment of VNIR-SWIR spectroscopy data is the key to establishing a high-precision inversion model. Integer-order derivatives (1.0-order, 2.0-order) are often used to preprocess soil VNIR-SWIR data because it can enhance the hyperspectral signals [9,10]. However, the original hyperspectral curve is quite different from the hyperspectral curve pretreated by a 1.0-order or 2.0-order derivative. Ignoring the gradual information of the three at different fractional-order derivative (FOD) levels [11] will lead to the loss of important hyperspectral information and affect the estimation accuracy of the inversion model. FOD expands the concept of integer-order derivative, which extends the order to any order. In recent years, a small number of scholars have used FOD to preprocess the indoor hyperspectral data of soils and extract more useful spectral information hidden in the fractional-order results, which can improve the accuracy of subsequent inversion models. For instance, Hong et al. [12] collected soil samples from a typical peri-urban agricultural area in Wuhan City (Hubei Province, China) and proposed a new FOD algorithm. An, ASD FieldSpec®3 portable spectrometer was used to measured spectra, which was done in a dark room. The lead (Pb) and zinc (Zn) concentrations of the samples were obtained in the laboratory and PLSR and random forest (RF) were used as calibration methods. This study demonstrated that the model accuracy of RF was better than PLSR, and the RF model for predict the concentration of Pb and Zn at 0.25- and 0.5-order had the optimal prediction accuracies. Zhang et al. [13] collected soil samples in northwestern China, and soil organic matter content (SOMC) and reflectance spectra were measured in the laboratory, FOD were used to pretreat soil spectra and a partial least squares-support vector machine (PLS-SVM) model was used to estimate SOMC. The conclusions showed that the 1.05- to 1.45-order range had the highest "signal-to-noise ratio", and it was most suitable for SOMC analysis. Wang et al. [14] used soil located at the Ebinur Lake Wetland National Nature Reserve (ELWNNR) in northwest China as research object. Three new FOD methods, the optimal remote sensing index and the subsection of spectral band method were selected to predict SOMC. Results showed that the optimal model appeared at 1.2-order, and its lowest root mean square error (RMSE) was 1.70 g/kg. Wang et al. [15] applied FOD was to the pretreatment of soil hyperspectral signals of samples collected from the Ebinur Lake basin in the Xinjiang Uighur Autonomous Region of China, and the PLSR model was used to estimate the clay content of the desert soils. Spectral reflectance and clay content were measured in the laboratory. Simulations showed that the 1.8-order FOD was effective.

At present, although some scholars use FOD to preprocess soil indoor hyperspectral signals, the indoor hyperspectral test environment is too ideal, and it can weaken the influence of the surrounding environment and weather on the hyperspectral data. In addition, the collected soil needs to be naturally air-dried, impurities must be-removed, the soil ground, sieved, leveled and other man-made operations applied before recording the indoor hyperspectral signals [16–18], which destroys the original porosity and water content of the soil, resulting in changes in the characteristics of the hyperspectral signals. The field hyperspectral are a true reflection of the soil growth environment, and their research value is greater. However, it is more difficult to collect field hyperspectra than indoor hyperspectra, and there are more external interference factors during the collection process, resulting in a lower "signal-to-noise ratio". At the same time, the collected field VNIR-SWIR is limited, and the amount of soil samples is small. However, although there are few reports on the processing of field spectroscopy data, there are still some scholars who provide good solutions to the problems existing in field spectroscopy measurements. For example, Ben-Dor et al. [19] developed a new assembly named Soil field PRObe (SoilPRO) for measuring the surface reflectance in the field, which was capable of measuring soil spectra in the field in a very precise and optimal manner that avoided most of the current soil-measurement problems experienced by users in the field, and the SP assembly was unique in that it eliminated the need for advanced planning and a reliance on independent environmental conditions. Francos et al. [20] developed a transfer function (TF) to predict the field spectral measurements from laboratory spectra and concluded that soil surface

reflectance values could be estimated based on laboratory spectra using a TF, which could assist in the processing of remote-sensing data and proximal sensing of surface properties.

In addition, stress caused by human activities such as farming, grazing, irrigation, development of wasteland, deforestation, etc. is a widespread interference phenomenon in Nature [21]. Unreasonable human activities lead to an increase in the groundwater level, which is strongly affected by surface evaporation, which will bring the bottom soil salt to the surface to accumulate, causing secondary salinization of the soil. At the same time, different human activity modes, degrees, and durations will affect the physical and chemical properties of the soil, and different degrees of human activity disturbances have different responses to soil water-soluble base ions. However, there are few reports on related studies in those areas.

Most of the research objects are soil samples collected in the same environment, and there are few published comparative analyses of the pretreatment effects for soil water-soluble base ions under different human interference environments. Therefore, this study collects VNIR-SWIR spectroscopy of soil samples from different human interference regions, preprocesses the soil VNIR-SWIR using FOD, observes the details of changes in the hyperspectral reflectance curve in different derivative, and verifies the feasibility of the application for FOD in the field hyperspectral under different degrees of human activity stress. The VNIR-SWIR spectroscopy of soil is measured by a ASDFieldSpec®3Hi-Res spectrometer in the field environment. This study provides a new method for the hyperspectral pretreatment of saline soils in different human interference areas, which has important practical significance for promoting the sustainable development of Xinjiang land resources, improving the saline soil in oases, and preventing further soil degradation.

2. Materials and Methods

2.1. Study Area

The study area is located at Fukang City (Changji Hui Autonomous Prefecture, Xinjiang Uygur Autonomous Region), and belongs to the alluvial fan margin of the Xinjiang 102 Corps southeast (87°44′E–88°46′E, 44°45′N–45°45′ N). Fukang has a typical mid-temperate continental arid climate. The winters are cold and long, the summers are hot and short, and the spring and autumn are not obvious. Sunight is abundant with about 2931.3 annual sunshine hours, and the temperature difference between day and night is large. The precipitation is scarce, as the average annual precipitation is about 164 mm, the evaporation is large (the annual average evaporation is about 2000 mm), the average annual frost-free period is about 170 days, the annual average temperature is about 6 °C. The natural environment with strong evaporation and scarce rainfall has made the problem of soil salinization in this area prominent, endangering the agricultural production and life of local residents.

Different degrees of human activity stress will have an impact on the ecological environment of oases. Based on the difference in the degree of soil interference by human activities, the test area is divided into three areas, namely, the lightly disturbed area (Area A) and the moderately disturbed area (Area B) and the severely disturbed area (Area C). Among them, the Area A is little affected by human interference, and its topography basically remains in its original state. Area B is moderately affected by human disturbance, the soil was mainly reclaimed around the 1950s and then abandoned. Area C is most affected by human disturbance, and it is mainly composed of two artificial forest lands. The distribution map of the study area and the soil sampling point map are shown in Figure 1.

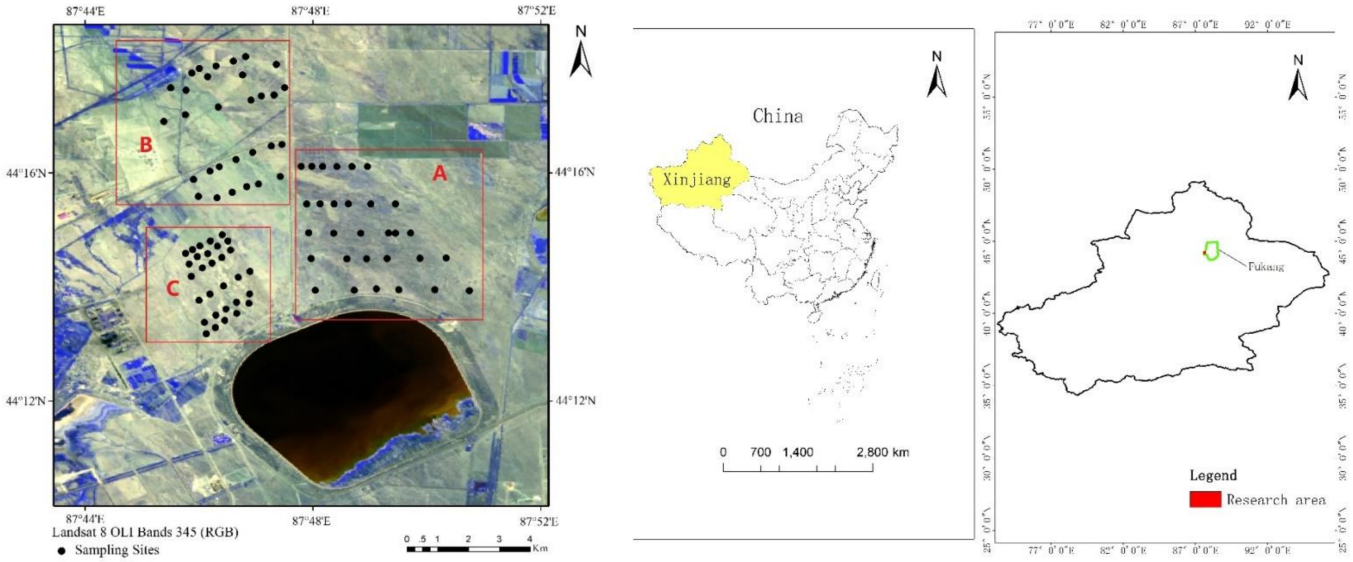

Figure 1. Distribution map of the study area and soil sampling point map.

2.2. Soil Sample Collection

The research team went to the field to collect soil samples in October 2017, and sampled them according to the location information of the 90 sampling points indicated in Figure 1. We choose a place with a flat terrain that can represent the average condition of the surrounding environment as the sampling point, and use the "Plum Blossom Pile" sampling method to select five soil samples with a size of 0–10 cm within 1 m around the sample point. After mixing them thoroughly, we put the composite sample in a sealed bag and marked the number, transporting them back to the laboratory for natural air drying, impurity removal, grinding, sieving and other operations, and then send them to the Xinjiang Institute of Ecology and Geography, Chinese Academy of Sciences for measuring soil Na^+ ion content by professionals. Atomic absorption spectrometry was used to determine the Na^+ content.

2.3. Soil Hyperspectra Collection

The soil field hyperspectra collection and soil sample collection were carried out at the same time and at the same place. The equipment used is an Analytical Spectral Device (ASD) FieldSpec®3Hi-Res spectrometer, and the wavelength range of the spectrometer is from 350 nm to 2500 nm. We measured the soil when the local time was 12:30–15:30, and the weather is sunny with little clouds and no wind. In addition, whiteboard correction is required before each collection, and each sample point is selected at five different locations within 1 m to repeat the measurements 10 times, and the average value of the 50 sets of hyperspectral curves is the measured field hyperspectral reflectance of this sample point. At the same time, the collected field VNIR-SWIR not only needs jumping point correction and Savitzky-Golay smoothing and denoising preprocessing, but the edge wavelength (350~399 nm and 2401~2500 nm) also needs to be removed the wavelength near the moisture absorption band (1340~1420 nm and 1800~1960 nm) are deleted, leaving 1759 hyperspectral wavelengths remaining.

2.4. Grünwald-Letnikov Fractional-Order Derivative

Fractional-order derivative (FOD) is a branch of mathematical theory which extends the order of integer derivative to any derivative, because it has the advantages of "memory" and "globality" [22–24], it can clearly describe the physical characteristics of the system and truly reveal the essential characteristics of the research object. At present, FOD is widely used in materials mechanics, digital filtering, system control, fractal theory, image processing, electromagnetic field theory and other fields [25,26].

Fractional calculus was first proposed by the great German philosopher, logician, mathematician, and scientist Gottfried Wilhelm Leibniz (1646–1716) in 1695. For more than 300 years, many mathematicians have worked hard in this field. A variety of definitions have appeared in the development of fractional calculus, such as Wely, Riemann-Liouville, Rize, Grünwald-Letnikov, Kolwankar-Gangal, Caputo, etc. [27,28]. Although the definition of fractional calculus is not uniform in terms of mathematical expression, it is mainly because different mathematicians consider different angles when analyzing and researching, and the forms obtained are naturally inconsistent. However, these formal processing methods have the same goal in different ways, they are both different and related, and they are equivalent under certain conditions. At present, three expressions of fractional calculus are often used, namely, Riemann-Liouville (R-L), Caputo, and Grünwald-Letnikov (G-L).

Euler's Gamma function is the basic function of fractional calculus. The integral form defined by Gamma function (also known as Euler second type integral) is as follows:

$$\Gamma(z) = \int_0^\infty e^{-t} t^{z-1} dt \tag{1}$$

The limit definition form of the complete Gamma function is:

$$\Gamma(z) = \lim_{n\to\infty} \frac{n! n^z}{z(z+1)\dots(z+n)} = \frac{1}{z} \prod_{k=1}^{\infty} \frac{\left(1+\frac{1}{k}\right)^z}{1+\frac{z}{k}} (z \neq n) \tag{2}$$

The definition of the incomplete Gamma function is:

$$\Gamma(c,z) = \frac{c^{-z}}{\Gamma(z)} \int_0^c t^{z-1} e^{-z} dt = e^{-z} \sum_{k-0}^{\infty} \frac{z^k}{\Gamma(k+c+1)} \tag{3}$$

Beta function is also called Euler first type integral, and its definition form is:

$$B(p,q) = \int_0^1 \tau^{p-1} (1-\tau)^{(q-1)} d\tau \tag{4}$$

The calculation formula of Grünwald-Letnikov FOD is written as follows:

$$dp_{f(X)} = \lim_{h\to 0} \frac{1}{h^p} \sum_{m=0}^{[(t-a)/h]} (-1)^m \frac{\Gamma(p+1)}{m!\Gamma(p-m+1)} f(X-mh) \tag{5}$$

where, p represents the order of the derivative, when it is a positive real number, and when it is a negative real number, p represents the order of integral. H represents the step length of derivative, t represents the upper limit of derivative, a represents the lower limit of derivative, and Γ represents the gamma function.

We assume that the function is a one-dimensional hyperspectral signal, and the range of the band is $[a, t]$, $x \in [a, t]$, and the band interval is divided equally according to the derivative step length. Because the resampling interval of the ASDFieldSpec®3Hi-Res spectrometer is 1 nm, and the derivative step length can be set h = 1. The difference expression of the FOD of the function can be derived from Equation (5) as follows:

$$\frac{dv_{f(X)}}{dX^v} \approx f(X) + (-v) f(X-1) + \dots + \frac{\Gamma(-\mathrm{v}+1)}{n!\Gamma(-\mathrm{v}+\mathrm{n}+1)} f(X-n) \tag{6}$$

where, v = 0 represents the 0.0-order derivative, that is no fractional differential processing is performed on the hyperspectral; v = 1 represents the integral-order 1.0-order derivative; v = 2 represents the integral-order 2.0-order derivative. In this paper, the preprocessing calculation of the FOD of hyperspectral signals is realized by programming in Matlab software.

2.5. Correlation Coefficient

The correlation coefficient is a method used in statistics to measure the degree of correlation between two variables, and the Pearson correlation coefficient method is commonly used. For two random variables (X and Y), there are several sets of data through experimental analysis, denoted as $(X_i, Y_i)(i = 1, 2, 3, \ldots, n)$, then the calculation of the correlation coefficient is shown in Equation (7):

$$r_{coor} = \frac{\sum_{i=1}^{n}(X_i - \overline{X})(Y_i - \overline{Y})}{\sqrt{\sum_{i=1}^{n}(X_i - \overline{X})^2 \sum_{i=1}^{n}(Y_i - \overline{Y})^2}} \quad (7)$$

where, $\overline{X} = n^{-1} \cdot \sum_{i=1}^{n} X_i$, represents the average value of all samples of the random variable X, and $\overline{y} = n^{-1} \cdot \sum_{i=1}^{n} Y_i$, represents the average value of all samples of the random variable Y.

The value range of the correlation coefficient r_{corr} is between -1 and $+1$. If the value of $|r_{corr}|$ is closer to 1, it indicates that the two random variables are more correlated. If $|r_{corr}| = 0$, it indicates that there is no correlation between the two random variables. When $|r_{corr}| \geq 0.8$, the two variables are highly correlated; when $0.5 \leq |r_{corr}| < 0.8$, the two variables are moderately correlated; when $0.3 \leq |r_{corr}| < 0.5$, the two variables are low-correlated; when $|r_{corr}| < 0.3$, it indicates that the correlation between the two variables is very weak, and it can be considered that the two variables are not correlated.

3. Simulation Results

3.1. Statistical Characteristics of Soil Salinity Information under Different Disturbance Degrees

We calculate the correlation of the three areas between the total salt content and water-soluble base ions (Na^+, K^+, Ca^{2+}, Mg^{2+}, Cl^-, SO_4^{2-}, CO_3^{2-}, HCO_3^-) (Tables 1–3), and give the values of the correlation coefficients in absolute values.

Table 1. Correlation coefficients between total salt and eight major ions in Area A.

Item	CO_3^{2-}	HCO_3^-	Cl^-	SO_4^{2-}	Ca^{2+}	Mg^{2+}	K^+	Na^+	Total Salt
CO_3^{2-}	1								
HCO_3^-	0.117	1							
Cl^-	0.241	0.379 *	1						
SO_4^{2-}	0.124	0.164	0.02	1					
Ca^{2+}	0.432 **	0.311 *	0.136	0.653 **	1				
Mg^{2+}	0.312 *	0.223	0.04	0.559 **	0.427 **	1			
K^+	0.025	0.124	0.035	0.017	0.353*	0.148	1		
Na^+	0.308 *	0.211	0.025	0.059	0.263	0.301	0.107	1	
total salt	0.158	0.051	0.155	0.527 **	0.309 *	−0.063	0.103	0.738 **	1

Note: * indicates a significant correlation at the 0.05 level. ** indicates a significant correlation at the 0.01 level.

Table 2. Correlation coefficients between total salt and eight major ions in Area B.

Item	CO_3^{2-}	$HCO_{3\_}$	Cl^-	SO_4^{2-}	Ca^{2+}	Mg^{2+}	K^+	Na^+	Total Salt
CO_3^{2-}	1								
$HCO_{3\_}$	0.336 *	1							
Cl^-	0.284	0.256	1						
SO_4^{2-}	0.029	0.086	0.036	1					
Ca^{2+}	0.629 **	0.579 **	0.523 **	0.330 *	1				
Mg^{2+}	0.376 *	0.393 *	0.598 **	0.063	0.493 **	1			
K^+	0.09	0.035	0.03	0.135	0.158	0.039	1		
Na^+	0.213	0.098	0.390 *	0.265	0.088	0.068	0.154	1	
total salt	0.007	−0.071	0.717 **	0.319 *	0.433 **	0.336 *	0.016	0.859 **	1

Note: * indicates a significant correlation at the 0.05 level. ** indicates a significant correlation at the 0.01 level.

Table 3. Correlation coefficients between total salt and eight major ions in Area C.

Item	CO_3^{2-}	HCO_3_	Cl^-	SO_4^{2-}	Ca^{2+}	Mg^{2+}	K^+	Na^+	Total Salt
CO_3^{2-}	1								
HCO_3_	0.112	1							
Cl^-	0.252	0.186	1						
SO_4^{2-}	0.278	0.448 **	0.573 **	1					
Ca^{2+}	0.361 *	0.474 **	0.574 **	0.801 **	1				
Mg^{2+}	0.186	0.477 **	0.119	0.335 *	0.461 **	1			
K^+	0.198	0.026	0.021	0.014	0.127	0.212	1		
Na^+	0.224	0.143	0.990 **	0.580 **	0.506 **	0.021	0.069	1	
total salt	0.269	0.238	0.979 **	0.697 **	0.685 **	0.124	0.026	0.971 **	1

Note: * indicates a significant correlation at the 0.05 level. ** indicates a significant correlation at the 0.01 level.

It can be seen from Table 1 that the correlation between total salt and Na^+ in Area A is better (0.738) and the correlation between total salt and SO_4^{2-} is better (0.527), while the correlation between total salt and Ca^{2+} is lower (0.309) and total salt and the remaining five ions (K^+,Mg^{2+},Cl^-,CO_3^{2-},HCO_3^-) have very low correlations. In addition, the correlation between SO_4^{2-} and Ca^{2+} is better (0.653), and the correlation between SO_4^{2-} and Mg^{2+} is good at 0.559, which indicates that there is more $CaSO_4$ and $MgSO_4$ in the soil of Area A. The correlation between CO_3^{2-} and Ca^{2+},CO_3^{2-} and Mg^{2+},CO_3^{2-} and Na^+,HCO_3^- and Ca^{2+} is general, and its value is about 0.3, which shows that there is also a certain amount of $CaCO_3$, $MgCO_3$, $NaCO_3$ and $CaHCO_3$ in the soil of Area A.

It can be seen from Table 2 that the correlation between total salt and Na^+ in Area B is better (0.859), the correlation between total salt and Cl^- is good at 0.717, the correlation between total salt and Ca^{2+} is general at 0.433, and the correlation between total salt and Mg^{2+} is less at 0.336, and the correlation between total salt and SO_4^{2-} is small at 0.319, and the correlation between total salt and the remaining three ions (K^+, CO_3^{2-}, HCO_3^-) is very low. At the same time, the correlation between CO_3^{2-} and Ca^{2+} is better (0.629), the correlation between HCO_3^- and Ca^{2+} is better (0.579), the correlation between Cl^- and Mg^{2+} is better (0.598), and the correlation between Cl^- and Ca^{2+} is better at 0.523, which shows that there is a lot of $CaCO_3$, $CaHCO_3$, MgCl and CaCl in the soil of Area B. The correlation between CO_3^{2-} and Mg^{2+} is general (0.376), the correlation between HCO_3^- and Mg^{2+} is general (0.393), the correlation between Cl^- and Na^+ is general at 0.390, and the correlation between SO_4^{2-} and Ca^{2+} is general at 0.330. It shows that there is also a certain amount of $MgCO_3$, $MgHCO_3$, NaCl and $CaSO_4$ in the soil of Area B.

It can be seen from Table 3 that the correlation between total salt and Cl^- and Na^+ in Area C is very good, reaching 0.979 and 0.971, respectively. The correlation between total salt and SO_4^{2-} is as good as 0.697, and the correlation between total salt and Ca^{2+} is also as good as 0.685, the correlation between the total salt and the remaining four ions (K^+, Mg^{2+}, CO_3^{2-}, HCO_3^-) is very low. At the same time, the correlation between Cl^- and Na^+ is 0.990, and the correlation between SO_4^{2-} and Ca^{2+} is 0.801, which indicates that there are a lot of NaCl and $CaSO_4$ in the soil of Area C. The correlation between Cl^- and Ca^{2+} is 0.574, and the correlation between SO_4^{2-} and Na^+ is 0.580, which shows that there is more CaCl and $NaSO_4$ in the soil of Area C. The correlation between HCO_3^- and Mg^{2+} is 0.477, the correlation between HCO_3^- and Ca^{2+} is 0.474, the correlation between CO_3^{2-} and Ca^{2+} is 0.361, and the correlation between SO_4^{2-} and Mg^{2+} is 0.335, so we can conclude there is a certain amount of $MgHCO_3$, $CaHCO_3$, $CaCO_3$ and $MgSO_4$.

The correlation analysis results of Tables 1–3 show that the total salt in Area B and C has a good correlation with Na^+ and Cl^- (the correlation is greater than 0.7), while the total salt in Area A only has a good correlation with Na^+.

3.2. Curve Characteristics of Soil Original Hyperspectral Reflectance Pretreated by FOD

In the MatLab software, the original hyperspectral reflectance curve (R) of the soil is subjected to FOD pretreatment, and the calculation process of the Grünwald-Letnikov

FOD in Equation (6) is realized through MatLab language programming. Among them, 0.1 is selected as the order interval of the FOD, 0.0-order is the starting order, and 2.0-order is the ending order. The characteristics of the original hyperspectral average reflectance curve of the soil in each interference area are shown in Figures 2–4. The abscissa represents the band range, and the ordinate represents the reflectance of the hyperspectral calculated by FOD. Because the number of all the bands of the hyperspectral is too large, and the difference of hyperspectral reflectance values processed by FOD within different orders is too large (Figures 2c,d, 3c,d and 4c,d), it is not easy to see the FOD characteristics of the hyperspectral reflectance curve. This article enlarges the local bands of 1.0-order to 1.5-order and 1.5-order to 2.0-order. In the front, middle, and back of the entire waveband range (350–2500 nm), 500–800 nm, 1450–1750 nm, and 2000–2300 nm are selected to discuss the hyperspectral reflectance of the soil in the lightly, moderately, and severe interference regions (Figures 2e,f, 3e,f and 4e,f).

In the three different interference regions, with the gradual increase of the orders, the reflectance derivative value of the ordinate gradually decreases, and it finally swings up and down at the derivative value of 0 (Figures 2–4). For example, the derivative value of the original hyperspectral reflectance of Area A ranges from 0.02 to 0.38 between 0.0-order and 0.5-order, and between 0.5-order and 1.0-order is 0.001 to 0.035, between 1.0-order and 1.5-order (Figure 1e) is -0.5×10^{-4}~10×10^{-4}, and the range between 1.5-order and 2.0-order (Figure 1f) is -1.25×10^{-4}~0.96×10^{-4}. The derivative value of the original hyperspectral reflectance of Area B ranges from 0.03 to 0.43 between 0.0-order and 0.5-order, and between 0.5-order and 1.0-order is 0.001 to 0.036, and between 1.0-order and 1.5-order (Figure 2e) is -8×10^{-4}~5×10^{-4}, and the range between 1.5- order and 2.0-order (Figure 2f) is -5.2×10^{-4}~0.9×10^{-4}. The derivative value of the original hyperspectral reflectance of Area C ranges from 0.03 to 0.49 between 0.0-order and 0.5-order, and from 0.5-order to 1.0-order is 0.001 to 0.043, and between 1.0-order and 1.5-order (Figure 3e) is -1.5×10^{-3}~2.23×10^{-3}, and the range between 1.5-order and 2.0-order (Figure 3f) is -1.4×10^{-3}~0.8×10^{-3}. The reason is that as the order of the fractional-order derivative gradually increases, the peak profile of the hyperspectral reflectance curve is gradually changed, and the peak removal operation is continuously completed, which causes the reflectance derivative value of the ordinate to gradually decrease.

3.3. The Correlation Coefficient between the Original Hyperspectral and Na^+ Is Affected by FOD

For soils with different degrees of human interference, the effect of FOD on the correlation coefficient between the original hyperspectral and Na^+ is shown in Figure 5. The simulation shows that when the correlation coefficients were in the light 0.0-order to 0.6-order, moderate 0.0-order to 0.4-order and severe 0.0-order to 0.4-order, none of the correlation coefficients in any band passed the 0.01 significance level test. When the order of the FOD is increased from 0.0-order to 1.0-order, the change trend of the correlation coefficient curve shows a certain gradual form. For example, the more obvious band range of the gradual change trend of the correlation coefficient curve is: 400–700 nm, 790–900 nm and 1200–1300 nm in the Area A; 400–950 nm, 1000–1300 nm and 1450–1750 nm in the Area B; and 400–900 nm, 1120–1330 nm and 1500–1780 nm in the Area C. However, when the order increases from 1.0-order to 2.0-order, the variation of the correlation coefficient curve fluctuates greatly, which is less obvious than the gradual change from 0.0-order to 1.0-order.

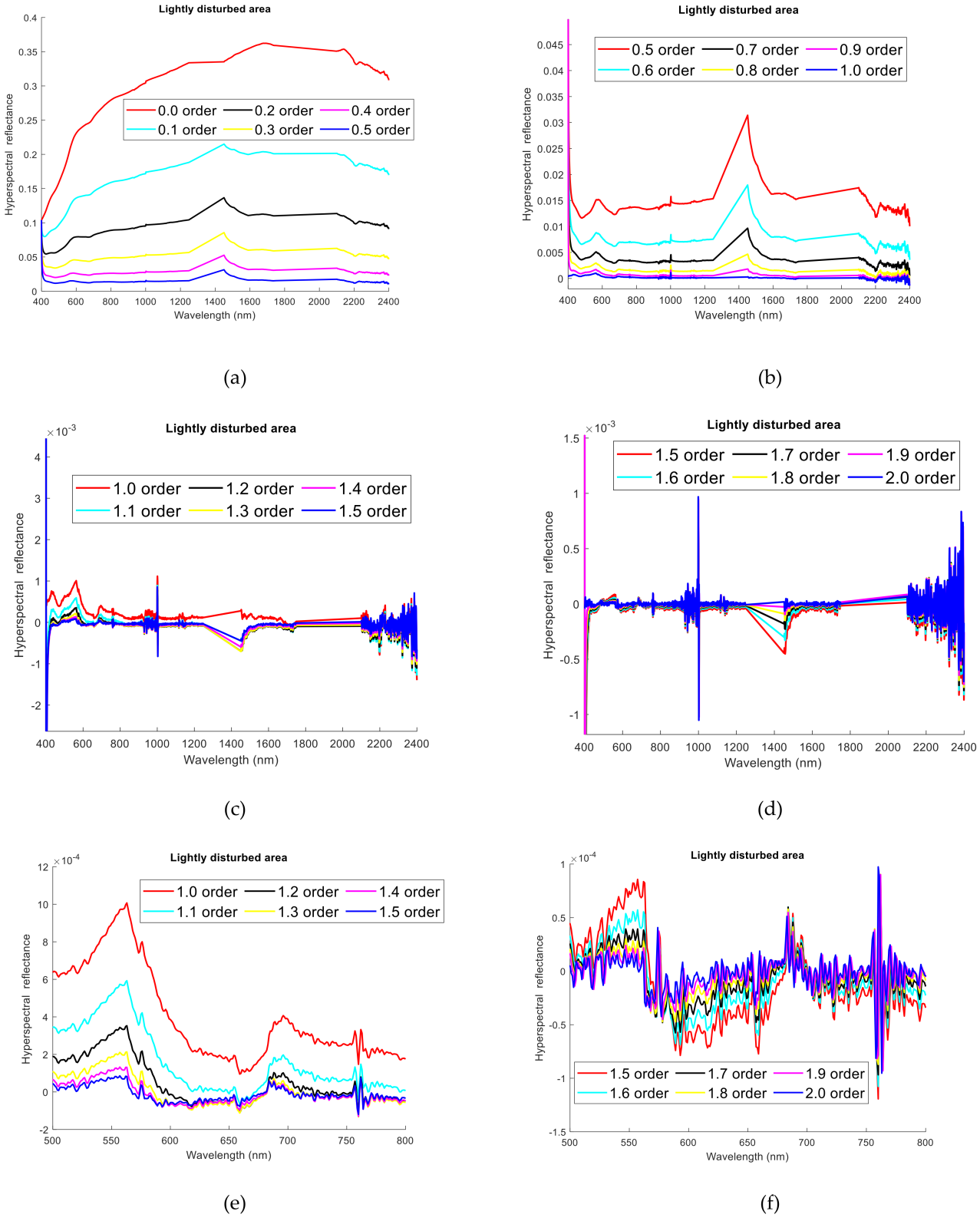

Figure 2. The reflectance curve of the soil original hyperspectral calculated by FOD in the lightly disturbed area: (**a**) 0.0-order to 0.5-order; (**b**) 0.5-order to 1.0-order; (**c**) 1.0-order to 1.5-order; (**d**) 1.5-order to 2.0-order; (**e**) 1.0-order to 1.5-order of local amplification band; (**f**) 1.5-order to 2.0-order of local amplification band.

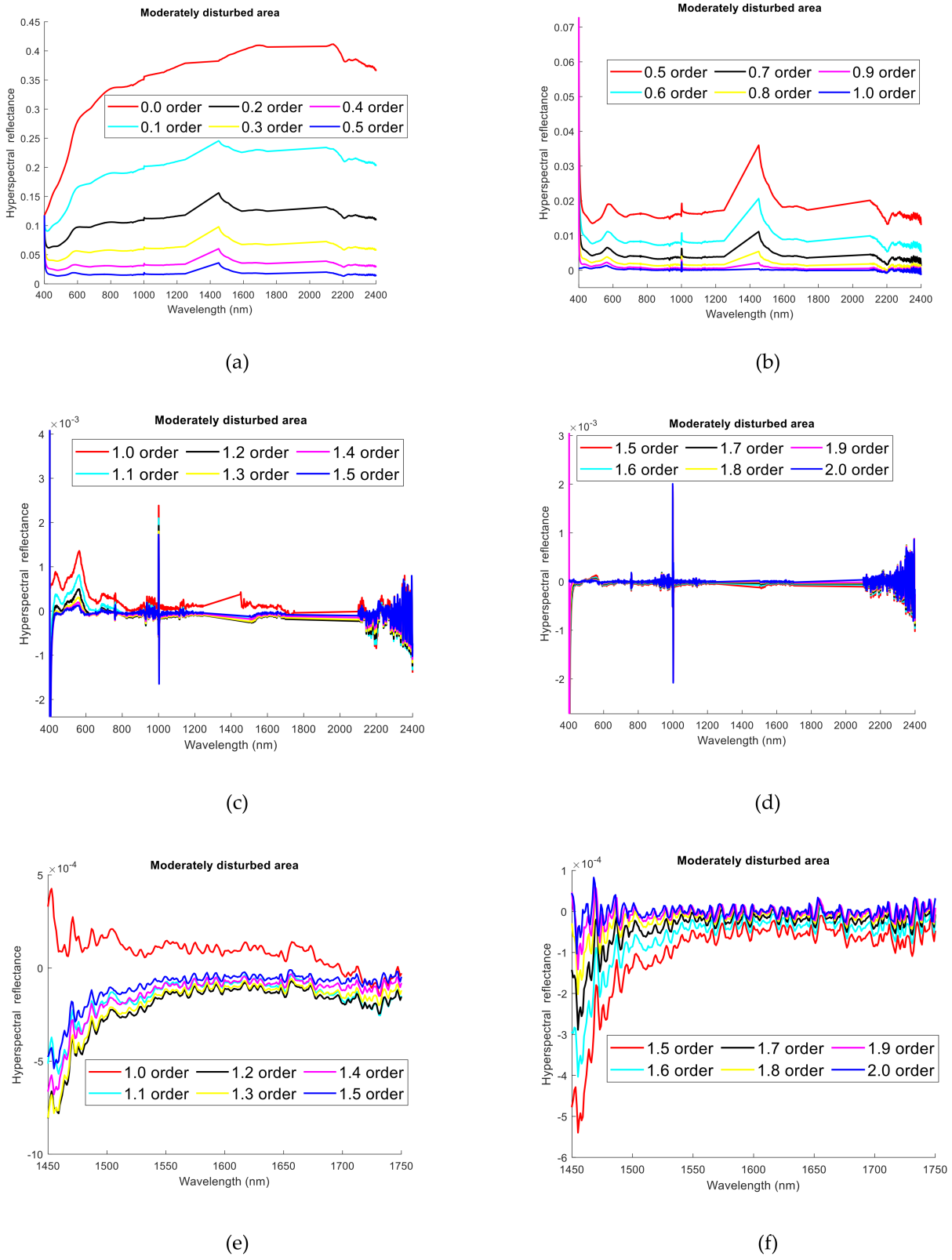

Figure 3. The reflectance curve of the soil original hyperspectral calculated by FOD in the moderately disturbed area: (**a**) 0.0-order to 0.5-order; (**b**) 0.5-order to 1.0-order; (**c**) 1.0-order to 1.5-order; (**d**) 1.5-order to 2.0-order; (**e**) 1.0-order to 1.5-order of local amplification band; (**f**) 1.5-order to 2.0-order of local amplification band.

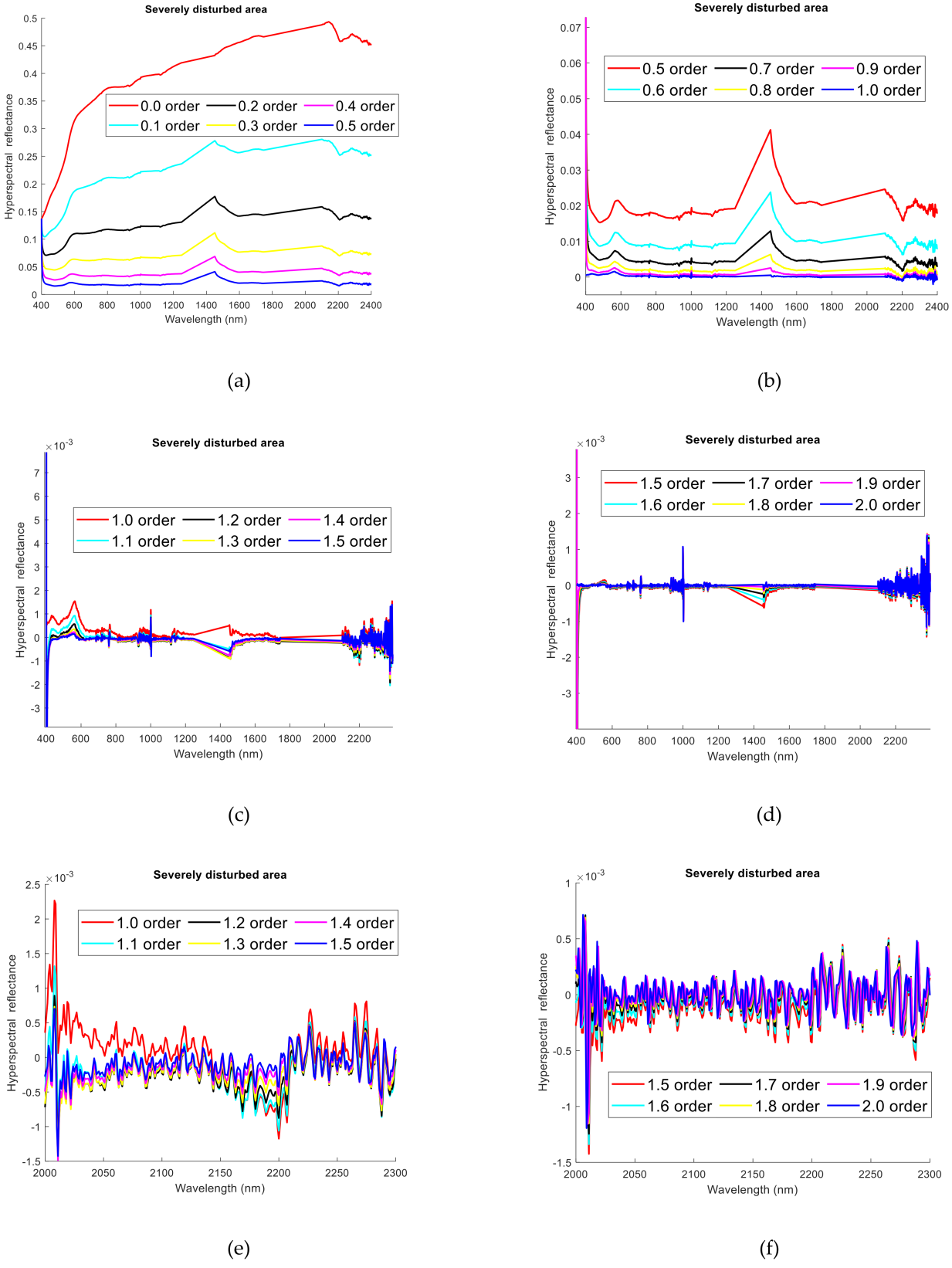

Figure 4. The reflectance curve of the soil original hyperspectral calculated by FOD in the severely disturbed area: (**a**) 0.0-order to 0.5-order; (**b**) 0.5-order to 1.0-order; (**c**) 1.0-order to 1.5-order; (**d**) 1.5-order to 2.0-order; (**e**) 1.0-order to 1.5-order of local amplification band; (**f**) 1.5-order to 2.0-order of local amplification band.

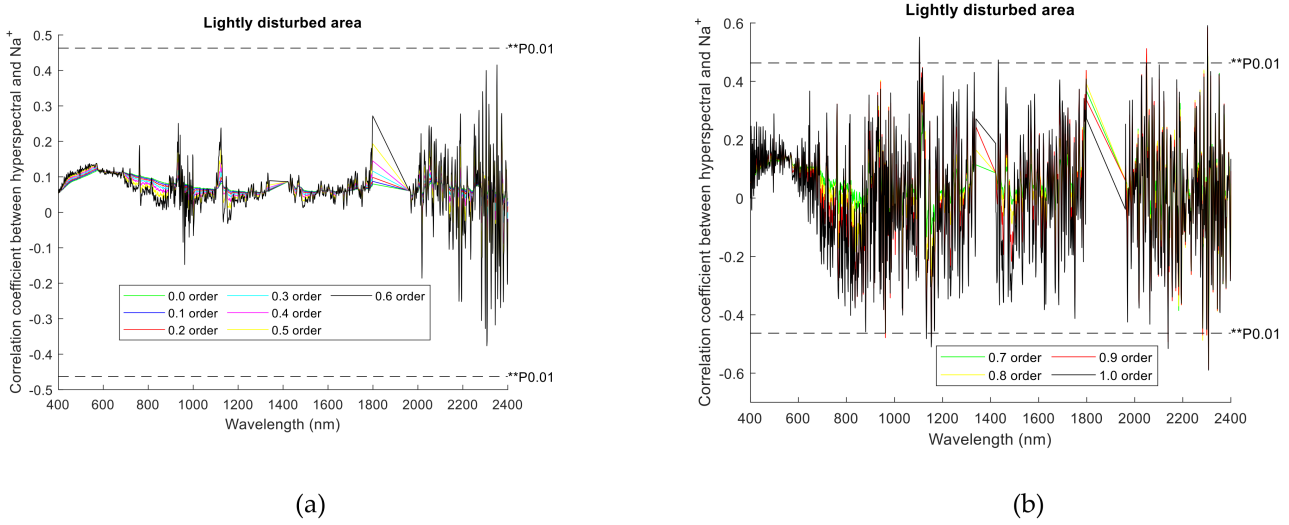

(a) (b)

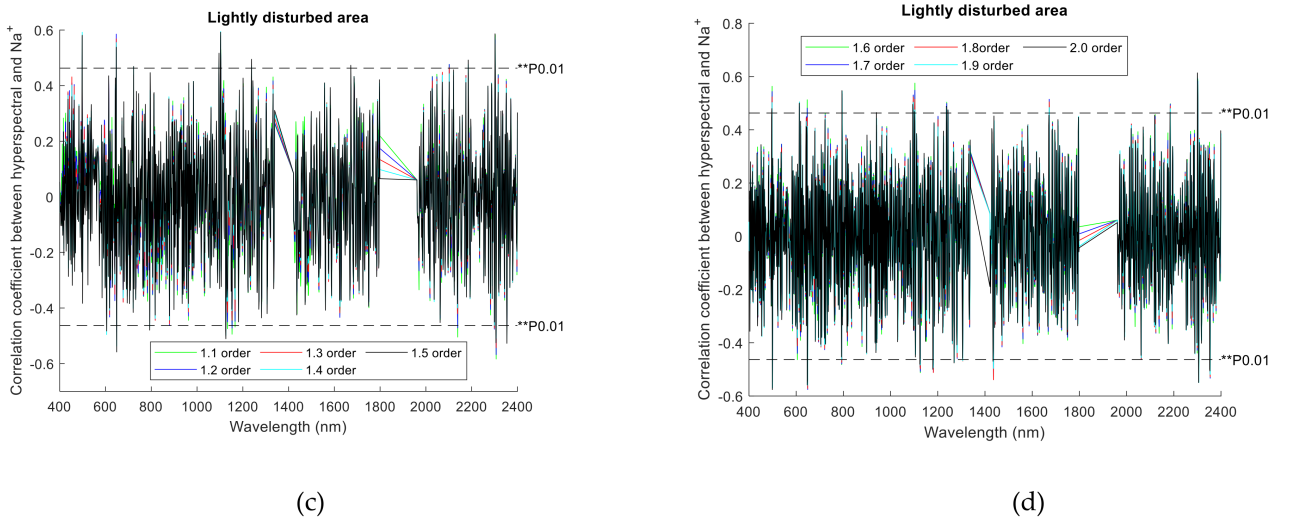

(c) (d)

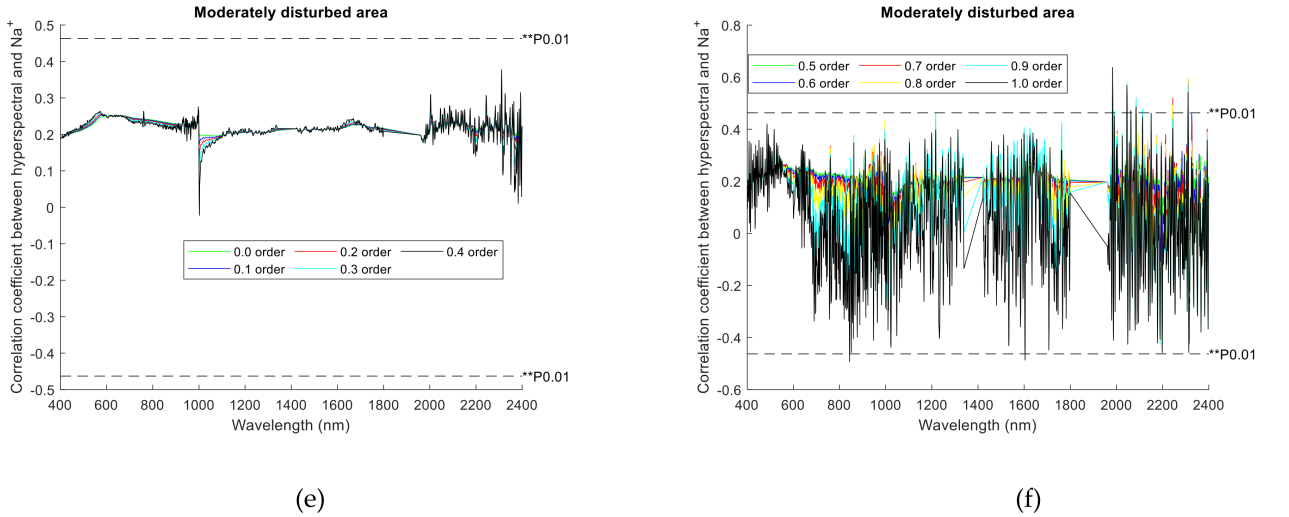

(e) (f)

Figure 5. *Cont.*

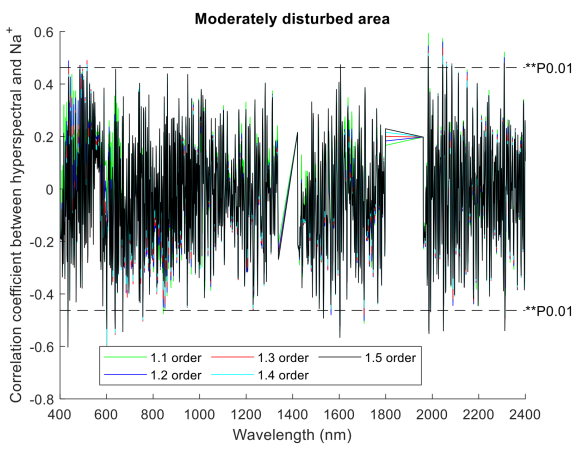

(g)

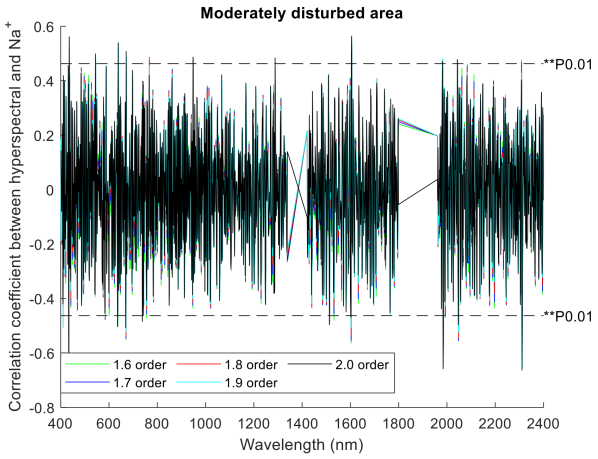

(h)

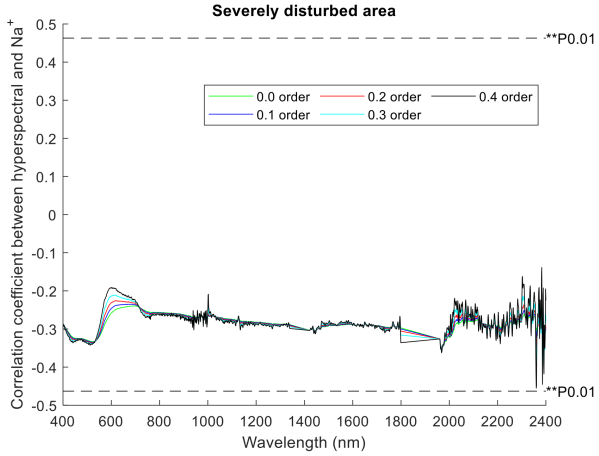

(i)

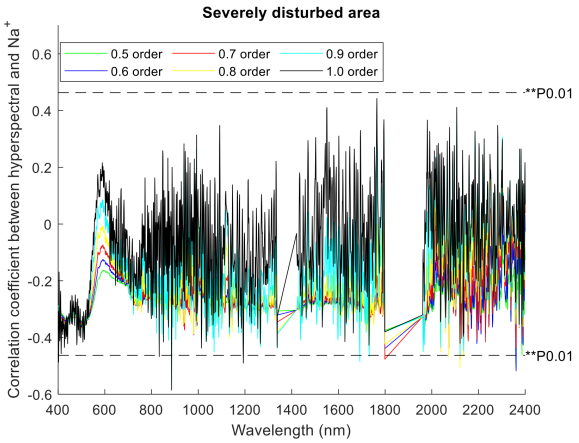

(j)

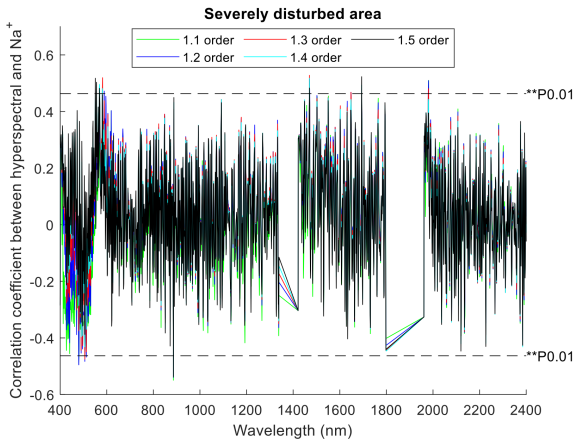

(k)

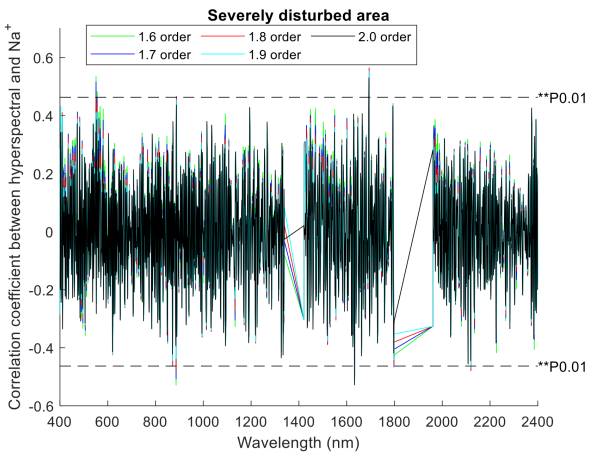

(l)

Figure 5. The correlation coefficient between soil hyperspectral and Na+ pretreated by FOD: (**a**) 0.0-order to 0.6-order in Area A; (**b**) 0.7-order to 1.0-order in Area A; (**c**) 1.1-order to 1.5-order in Area A; (**d**) 1.6-order to 2.0-order Area A. (**e**) 0.0-order to 0.4-order in Area B; (**f**) 0.5-order to 1.0-order in Area B; (**g**) 1.1-order to 1.5-order in Area B; (**h**) 1.6-order to 2.0-order in Area B. (**i**) 0.0-order to 0.4-order in Area C; (**j**) 0.5-order to 1.0-order in Area C; (**k**) 1.1-order to 1.5-order in Area C; (**l**) 1.6-order to 2.0-order in Area C.

There are certain differences in the shape of the correlation coefficient curve in different FOD. Regardless of the area of human interference, the correlation coefficient curve is shown that the outline is clearer in the low-order derivative (order 0.0–0.4), and the trend of change is relatively gentle. In addition, for the hyperspectral data without FOD pretreatment (it is 0.0-order), the correlation coefficient ranges are very small, and show different positive and negative correlations in each area, such as 0.0330~0.1175 in Area A, 0.1843~0.2512 in Area B, and −0.3514~−0.2395 in Area C.

In addition, Figure 5 also shows that the FOD pretreatment can improve the correlation coefficient between the original hyperspectral and Na^+. For example, in the Area A, the 0.2-order is −0.0101~0.1255, the 0.5-order is −0.2350~0.3557, the 0.7-order is −0.5105~0.4855, the 0.9-order is −0.5861~0.5848, the 1.2-order is −0.5678~0.5853, the 1.5-order is −0.5580~0.5921, and the 1.9-order is −0.5692~0.5940. In Area B, the order of 0.3 is 0.0685~0.3147, the order of 0.5 is −0.1196~0.4758, the order of 0.8 is −0.4290~0.5942, the order of 1.1 is −0.5183~0.5933, the order of 1.4 is −0.5961~0.5170, and the order of 1.7 is −0.6589~0.5262. In Area C, the order of 0.3 is −0.3966~−0.2111, the order of 0.5 is −0.5094~−0.0205, the order of 0.8 is −0.5058~0.2962, the order of 1.1 is −0.5494~0.5102, the order of 1.4 is −0.5406~0.5178, and the order of 1.7 is- 0.5075~0.5612. Therefore, with the increase of the FOD, the overall variation range of the correlation coefficient between the original hyperspectral and Na^+ is gradually increased.

3.4. The Correlation Coefficient between Each Spectra and Na^+ Passed the 0.01 Test under Different Derivative

In the original spectrum and its transformation spectrum, many of the bands that passed the 0.01 test appear in the fractional order, but the FOD and the band numbers have certain differences in each spectrum (R, $\sqrt{R}$, 1/R, lgR, 1/lgR). For example, the sequence of the band numbers in Area A under the different FOD from large to small is: 30 band numbers in lgR of 1.9-order > 28 band numbers in $\sqrt{R}$ of 1.8-order > 27 band numbers in R of 1.8-order > 25 band numbers in 1/R of 1.9-order> 19 band numbers in 1/lgR of 1.8- and 1.9-order. In Area B that is 25 band number in 1/lgR of 1.5-order > 20 band numbers in R of 1.3- and 1.8-order > 19 band numbers in $\sqrt{R}$ of 1.3-order > 18 band numbers in lgR of 1.3- and 1.4-order > 15 band numbers in 1/R of 1.5-order. In Area C that is 98 band numbers in 1/R of 0.8-order > 76 band numbers in lgR of 1-order > 26 band numbers in $\sqrt{R}$ of 1.2-order > 10 band numbers in R of 1.2-order > 2 band numbers in 1/lgR of 1.2-order.

We count the number of bands where the correlation coefficient between different spectral transformations and Na^+ passed the 0.01 test pretreated by FOD. In each spectrum, there are many FOD band numbers that exceed the integer-order, and they are concentrated in higher-order FOD derivative (1.2- to 1.6-ordder). For example, the band numbers of FOD are more than integer 1.0-order, it mainly appears in the 1.4- to1.9-order of each spectrum in the Area A, it mainly appears in the 1.2- to1.9-order of each spectrum in the Area B, while in the Area C it mainly appears in the R and $\sqrt{R}$ from 1.2- to 1.6-order, in the 1/R from 0.6- to 0.9-order or 1.2- to 1.3-order.

Whereas it can been seen that the band numbers of FOD are more than integer 2.0-order from Figure 6, it mainly appears in the 1.7- to 1.9-order of each spectrum in the Area A, it mainly appears in the 1.3- to 1.9-order of each spectrum in the Area B, and in the Area C it mainly appears in R, $\sqrt{R}$, 1/R of 0.9- to 1.1-order, as well as 1.2-order of 1/lgR.

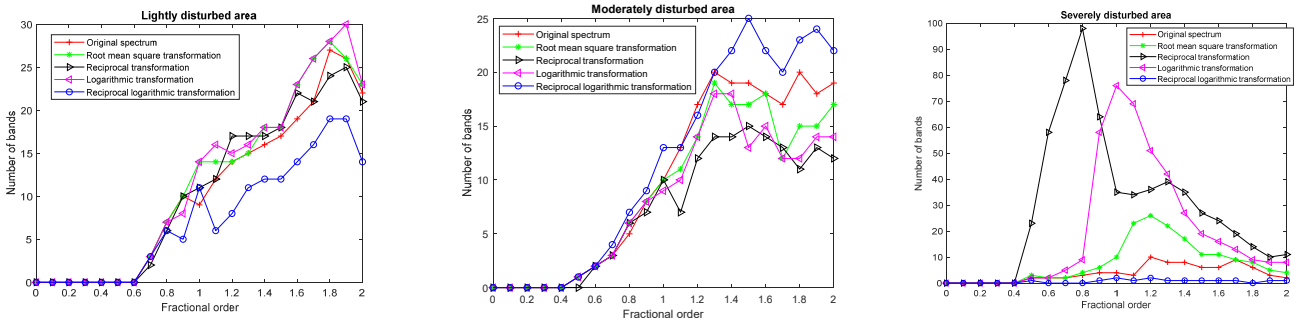

(a) (b) (c)

Figure 6. The number of bands where the correlation coefficient between each spectral transformation and Na^+ passed the 0.01 test: (**a**) Area A, (**b**) Area B, (**c**) Area C.

3.5. The Maximum Correlation Coefficient between Each Spectrum and Na^+ Pretreated by FOD

We analyze the absolute value of the maximum correlation coefficient between each spectrum and Na^+, as well as its corresponding fractional-order and band (Tables 4–6). Overall, with the increase of the FOD, the absolute value of the maximum correlation coefficient of each spectrum at different orders shows a trend of first increasing and then decreasing, and the improvement of the correlation coefficient by the low-order derivative is small. While the improvement of the correlation coefficient by the higher-order derivative is great, for example, 1.4- and 1.5-order in Area A, 1.8- and 1.9-order in Area B, and 1.0- to 1.8-order in Area C.

Table 4. The absolute value of the maximum correlation coefficient between the hyperspectral and Na^+ in Area A and its corresponding band.

Order	R		$\sqrt{R}$		1/R		lgR		1/lgR	
	Band/nm	Max Value	Band/nm	Max Value	Band/nm	Max Value	Band/nm	Max Value	Band/nm	Max Value
0.0	572	0.1175	572	0.1253	584	0.1502	572	0.1334	572	0.1138
0.1	572	0.1206	571	0.1291	571	0.1565	571	0.1380	572	0.1161
0.2	2352	0.1255	571	0.1333	570	0.1646	571	0.1432	2352	0.1210
0.3	2352	0.1768	2352	0.1808	2352	0.1935	2352	0.1850	2352	0.1735
0.4	2352	0.2593	2352	0.2606	2352	0.2637	2352	0.2618	2352	0.2608
0.5	2352	0.3557	2352	0.3531	2352	0.3415	2352	0.3499	2352	0.3621
0.6	2352	0.4156	2352	0.4137	2352	0.3966	2352	0.4098	2352	0.4153
0.7	2307	0.5105	2307	0.4968	2303	0.4832	2303	0.4845	2307	0.5118
0.8	2307	0.5671	2303	0.5665	2303	0.5835	2303	0.5768	2307	0.5432
0.9	2307	0.5861	2303	0.6002	2303	0.6246	2303	0.6122	2307	0.5550
1.0	2303	0.5911	2303	0.6061	2303	0.6311	2303	0.6179	2307	0.5610
1.1	2307	0.5835	2303	0.5970	2303	0.6197	2303	0.6078	2307	0.5614
1.2	647	0.5853	498	0.5947	2303	0.5963	2303	0.5867	2307	0.5548
1.3	1103	0.5797	498	0.5934	1103	0.5937	1103	0.5942	1103	0.5570
1.4	1103	0.5948	1103	0.6081	1103	0.6276	1103	0.6184	498	0.5716
1.5	1103	0.5921	1103	0.6070	1103	0.6335	1103	0.6193	498	0.5721
1.6	2302	0.5888	2302	0.6022	1103	0.6201	2302	0.6097	498	0.5593
1.7	2302	0.5826	2302	0.5995	2302	0.6117	2302	0.6098	649	0.5576
1.8	649	0.5715	2302	0.5904	2302	0.6119	2302	0.6044	649	0.5531
1.9	2301	0.5940	2301	0.5961	2302	0.6085	2302	0.5941	2301	0.5770
2.0	2300	0.5912	2300	0.6014	2301	0.6016	2300	0.6134	2300	0.5712

Table 5. The absolute value of the maximum correlation coefficient between the hyperspectral and Na^+ in Area B and its corresponding band.

Order	R		$\sqrt{R}$		1/R		lgR		1/lgR	
	Band/nm	Max Value	Band/nm	Max Value	Band/nm	Max Value	Band/nm	Max Value	Band/nm	Max Value
0.0	661	0.2512	661	0.2329	574	0.1660	591	0.2122	2311	0.2744
0.1	2311	0.2562	2311	0.2400	2311	0.1773	2311	0.2214	2311	0.2857
0.2	2311	0.2777	2311	0.2623	2311	0.2018	2311	0.2445	2311	0.3050
0.3	2311	0.3147	2311	0.3008	2311	0.2448	2311	0.2844	2311	0.3375
0.4	2311	0.3777	2311	0.3669	2311	0.3211	2311	0.3538	2311	0.3916
0.5	2311	0.4758	2311	0.4717	2311	0.4493	2311	0.4656	2311	0.4720
0.6	2311	0.5715	2311	0.5771	2311	0.5834	2311	0.5807	2311	0.5454
0.7	2310	0.5942	2310	0.6081	2310	0.6090	2310	0.6164	2310	0.5375
0.8	2310	0.5942	2310	0.6005	2310	0.5683	2310	0.5989	2310	0.5530
0.9	2046	0.5803	2046	0.5781	2046	0.5671	2046	0.5751	2046	0.5774
1.0	1983	0.6373	1983	0.6255	1983	0.5430	1983	0.6035	1983	0.5924
1.1	1983	0.5933	2045	0.5643	2045	0.5368	2045	0.5546	1983	0.5976
1.2	2045	0.5609	2045	0.5527	2045	0.5321	2045	0.5450	2045	0.5863
1.3	601	0.6064	601	0.6142	1603	0.5357	601	0.6103	2045	0.5653
1.4	601	0.5961	601	0.5779	1603	0.5558	1603	0.5622	601	0.6060
1.5	434	0.6026	434	0.6082	1603	0.5594	434	0.5887	434	0.5933
1.6	434	0.6371	434	0.6412	434	0.5842	434	0.6311	434	0.6300
1.7	434	0.6589	434	0.6589	434	0.6155	434	0.6504	434	0.6536
1.8	434	0.6726	434	0.6665	434	0.6113	434	0.6538	434	0.6691
1.9	434	0.6820	434	0.6699	434	0.5969	434	0.6516	434	0.6800
2.0	433	0.6801	433	0.6627	2311	0.5912	433	0.6496	433	0.6796

Table 6. The absolute value of the maximum correlation coefficient between the hyperspectral and Na^+ in Area C and its corresponding band.

Order	R		$\sqrt{R}$		1/R		lgR		1/lgR	
	Band/nm	Max Value	Band/nm	Max Value	Band/nm	Max Value	Band/nm	Max Value	Band/nm	Max Value
0.0	1969	0.3514	1969	0.3588	1969	0.3694	1969	0.3643	522	0.3300
0.1	1969	0.3531	1969	0.3607	1969	0.3719	1969	0.3664	514	0.3311
0.2	2392	0.3556	1969	0.3630	1969	0.3747	1969	0.3689	2386	0.3365
0.3	2386	0.3966	2360	0.4012	2392	0.4114	2360	0.4059	2386	0.3832
0.4	2360	0.4552	2360	0.4593	2360	0.4621	2360	0.4619	2360	0.4449
0.5	2361	0.5094	2361	0.5130	570	0.5208	2361	0.5151	2361	0.4873
0.6	2361	0.5175	2361	0.5263	592	0.5493	2361	0.5322	2230	0.3660
0.7	2121	0.4772	2121	0.4866	592	0.5322	2121	0.4922	2121	0.3904
0.8	2121	0.5058	2121	0.5073	632	0.5412	2137	0.5090	2121	0.4245
0.9	886	0.5555	886	0.5802	886	0.6325	886	0.6017	886	0.4832
1.0	886	0.5521	886	0.5971	886	0.6022	556	0.6364	886	0.5098
1.1	886	0.5494	886	0.5544	1632	0.5686	556	0.6377	886	0.5189
1.2	886	0.5338	556	0.5907	1470	0.5682	555	0.6459	480	0.5068
1.3	886	0.5359	556	0.6204	1470	0.5925	555	0.6594	886	0.5094
1.4	886	0.5406	555	0.6175	1470	0.6043	555	0.6680	886	0.5146
1.5	886	0.5392	555	0.6146	555	0.6140	555	0.6577	886	0.5141
1.6	1694	0.5466	551	0.5844	1694	0.6241	555	0.6172	886	0.5045
1.7	1694	0.5612	1694	0.5837	1694	0.6265	1694	0.6017	886	0.4849
1.8	1694	0.5644	1694	0.5826	1694	0.6203	1694	0.5978	886	0.4558
1.9	1694	0.5542	1694	0.5698	1694	0.6061	1694	0.5836	1694	0.4748
2.0	1693	0.5300	1633	0.5516	1633	0.5927	1633	0.5698	1693	0.4761

In addition, the maximum correlation coefficient of each spectrum appears in the fractional order under different FOD, such as, the absolute value of the maximum correlation

coefficient for five spectrum (R, $\sqrt{R}$, 1/R, lgR, 1/lgR) and its corresponding fractional-order and band in Area A are 0.5948 and 1.4-order of 1103 nm, 0.6081 and 1.4-order of 1103 nm, 0.6335 and 1.5-order of 1103 nm, 0.6193 and 1.5-order of 1103 nm, 0.5770 and 1.9-order of 2301 nm, respectively. They are 0.6820 and 1.9-order of 434 nm, 0.6699 and 1.9-order of 434 nm, 0.6155 and 1.7-order of 434 nm, 0.6538 and 1.8-order of 434 nm, 0.6800 and 1.9-order of 434 nm, respectively in the Area B. While they are 0.5644 and 1.8-order of 1694 nm, 0.6204 and 1.3-order of 556 nm, 0.6265 and 1.7-order of 1694 nm, 0.6680 and 1.4-order of 555 nm, 0.5189 and 1.1-order of 886 nm, respectively in the Area C.

Therefore, whether it is the original hyperspectral or the transformed hyperspectral under different human interference areas, the absolute value of the maximum correlation coefficient between the hyperspectral reflectance of each spectrum and the cation Na+ appears in the FOD, and its corresponding bands in Area A are 1103 nm (R, $\sqrt{R}$, 1/R, lgR) and 2301 nm (1/lgR), and they appear in 1.4-, 1.5-, 1.9-orders. In Area B they are 434 nm (R, $\sqrt{R}$, 1/R, lgR, 1/lgR), and they appear in 1.7-, 1.8-, and 1.9-orders. While in the Area C they are 555 nm (lgR), 556 nm ($\sqrt{R}$), 886 nm (1/lgR) and 1694 nm (R, 1/R), and they appear in 1.1-, 1.3-, 1.4-, 1.7-, 1.8-orders (Tables 4–6).

4. Discussion

4.1. Fractional-Order Derivative Improves the Resolution between Hyperspectral Peaks

In the derivation calculation process of the FOD, the derivation calculation itself is a method to increase the resolution of the spectral signal, and the selection of the order has the characteristics of continuity, so the detailed change process of the derivative value of the hyperspectral reflectance can be accurately displayed, and the resolution between the peaks of the spectrum can be improved. For example, as the order increases, the peaks and valleys in the hyperspectral reflectance curve become more and more obvious (Figures 1–3).

FOD is a derivative that extends the integer-order to any order. Because of its advantages of "memory" and "globality", it can more clearly describe the physical characteristics of the system, and reveal the non-linear characteristics and variation laws of the field hyperspectra of saline soil. That is, when the order of FOD increases from 0.0-order to 1.0-order, the hyperspectral reflectance curve of each order slowly approaches the 1.0-order hyperspectral reflectance curve, and the result of the derivate value reflects the increased sensitivity to the slope of the hyperspectral reflectance curve. While the order of the FOD is increased from 1.0-order to 2.0-order, the hyperspectral reflectance curve of each order slowly approaches the 2.0-order hyperspectral reflectance curve, and the result of the differential value reflects the increased sensitivity to the curvature of the hyperspectral reflectance curve. Therefore, the former describes various changes from 0.0-order derivation to 1.0-order derivation, and the latter describes in more detail the subtle difference between the slope and curvature of the hyperspectral reflectance curve. This further illustrates that FOD calculation can enhance the pretreatment effect of soil field hyperspectral data, improve the resolution between hyperspectral peaks, and highlight the "sensitivity" characteristics of FOD.

In addition, as far as this research is concerned, we compare and analyze the change law of the correlation coefficient of each derivative for each transformation and the influence of the derivative processing on the correlation coefficient, which can explore the application value of fractional-order derivatives in hyperspectral data preprocessing.

4.2. Comparison of the Fractional-order derivative and Integer-order derivative

According to the theory of integer-order derivatives, the first derivative of the differentiable function $f(X)$ is defined as:

$$f'_{(X)} = \lim_{h \to 0} \frac{f(X) - f(X-h)}{h} \tag{8}$$

The second derivative of the function $f(X)$ is defined as:

$$f''_{(X)} = \lim_{h\to 0} \frac{f(X) \ - \ 2f(X-h) \ + \ f(X-2h)}{h^2} \tag{9}$$

The third derivative of the function $f(X)$ is defined as:

$$f'''_{(X)} = \lim_{h\to 0} \frac{f(X) \ - \ 3f(X-h) + 3f(X-2h) - f(X-3h)}{h^3} \tag{10}$$

If the derivative order of the function $f(X)$ is increased to a higher-order n, then the n-order derivative of the function $f(X)$ can be written as follows:

$$f(n)_{(X)} = \lim_{h\to 0} \frac{1}{h^n} \sum_{m=0}^{n} (-1)^m \begin{pmatrix} n \\ m \end{pmatrix} f(X-mh) \tag{11}$$

If the gamma function is used to replace the binomial coefficients of Formula (11), and the derivative order is extended to a non-integer order, then the Grünwald-Letnikov fractional derivative (Equation (5)) can be obtained.

It can be seen from the derivation of the above formula that the FOD extends the order to a non-integer order, generalizing the definition of the derivative, and when the derivative order is a positive integer, the integer-order derivative becomes a special case of the FOD. In the numerical calculation process, the integer-order derivative is only related to the information of the points in the derivative window, and has nothing to do with the points far away. While the FOD is not only related to the value of this point, but also related to the value of all points before this point.

For the fractional-order derivative, it can be seen from Equation (6) that the value of the v-order FOD of the function *f(X)* in a certain waveband is not only related to the hyperspectral reflectance *f(X)* of this waveband, but also related to the previous wavebands, namely, it is related to *f(X−1)*, *f(X−2)*, *f(X−3)*, . . . , *f(X-n)*. This phenomenon shows that the closer the point is, the greater the weight and the impact is. On the contrary, the farther the point is, the smaller the weight, and the influence also decreases. These are the well-known "memory" and "non-locality" of the FOD. It is also the biggest difference between the fractional-order derivative and the integer-order derivative [29–32].

In addition, the order choice of FOD is not limited to integers, and the order of operations is expanded [33–36], which has a wider selection range and higher degree of freedom than integer-order derivatives. Meanwhile, many systems belong to the fractional-order, and the integer-order derivative model is used to describe it, which will lead to a large deviation between the model and the actual result, and the system simulation and prediction cannot be performed well, it also ignores the authenticity of the system to a certain extent.

4.3. The Percentage Improvement of the Fractional-Order Maximum Correlation Coefficient Compared with the Integer-Order

Compared with the absolute value of the maximum correlation coefficient of integer-order, the percentage increase of the absolute value of the maximum correlation coefficient of fractional-order in each spectrum is studied (Table 7). From Tables 4–6, it can be seen that the fractional-order where the maximum correlation coefficient between the five transform spectra and the cation Na^+ is located is 1.4-, 1.5-, 1.9-orders in Area A, and 1.7-, 1.8-orders in Area B, and 1.1-, 1.3-, 1.4-, 1.7-, 1.8-orders in Area C.

Table 7. The absolute value of the fractional-order maximum correlation coefficient is greater than the absolute value of the integer-order maximum correlation coefficient (correlation coefficient improvement percentage).

Spectrum	The Fractional-Order where the Largest Correlation Coefficient Is Located	Greater Than Integer 1.0-Order			Greater Than Integer 2.0-Order		
		Area A	Area B	Area C	Area A	Area B	Area C
R	1.4 order of Area A, 1.9 order of Area B,1.8 order of Area C	0.63%	7.01%	2.23%	0.61%	0.28%	6.49%
$\sqrt{R}$	1.5 order of Area A, 1.9 order of Area B, 1.3 order of Area C	0.33%	7.10%	3.90%	1.11%	1.09%	12.47%
1/R	1.5 order of Area A, 1.7 order of Area B, 1.7 order of Area C	0.38%	13.35%	4.04%	5.30%	4.11%	5.70%
lgR	1.5 order of Area A, 1.8 order of Area B, 1.4 order of Area C	0.23%	8.33%	4.97%	0.96%	0.65%	17.23%
1/lgR	1.9 order of Area A, 1.9 order of Area B, 1.1 order of Area C	2.85%	14.79%	1.79%	1.02%	0.06%	8.99%

Note: Correlation coefficient promotion % = (xx − yy)/yy, xx represents the absolute value of the maximum correlation coefficient of the fractional-order in different transformations, and yy represents the absolute value of the maximum correlation coefficient of the integer-order in different transformations.

Compared with the integer-order 1.0-order, the fractional improvement percentages of the five spectra are all greater than 0.22% in the Area A, greater than 7% in the Area B, and greater than 1.7% in the Area C. Among them, the 1.9-order of 1/lgR transformation has the largest increase percentage in Area A, which is 2.85%; the 1.9-order of 1/lgR transformation has the largest increase percentage in Area B, which is 14.79%; the 1.4-order of lgR transformation has the largest increase percentage in Area C, which is 4.97%.

Compared with the integer-order 2.0-order, the fractional improvement percentages of the five spectra are all greater than 0.6% in the Area A, greater than 0.05% in the Area B, and greater than 5.5% in the Area C. Among them, the 1.5-order of 1/R conversion in the Area A has a maximum increase of 5.30%; the 1.7-order of 1/R conversion in Area B has a maximum increase of 4.11%; the 1.4-order of lgR conversion in the Area C has a maximum increase of 17.23%.

Regardless of whether it is compared with the 1.0-order or the 2.0-order integer-order, the percentage of increase in the absolute value of the maximum correlation coefficient between the FOD and the cation Na^+ in the three regions is mostly more than 3%, and the highest is more than 17%. It can be seen that the effect of the fractional-order on the correlation between hyperspectral and cation Na^+ is significantly better than that of the integer-order.

4.4. The Advantages of Different Transform Spectra

The advantages of different transform spectra are as follows:

We perform non-linear mathematical transformation on the original spectral reflectance (R). Non-linear mathematical transformations that are often used mainly include: root mean square transformation ($\sqrt{R}$), reciprocal transformation (1/R), logarithmic transformation (lgR), logarithm reciprocal transformation (1/lgR). The main purpose of this implementation is as follows:

On the one hand, the purpose of introducing these spectral transformation forms is to enrich spectral data, increase the sensitivity of spectral data to the properties of the soil to be tested, and improve the correlation between the spectral data and soil property, so that the relationship between the data can be found more conveniently.

On the other hand, the implementation of nonlinear transformation can enhance the spectral difference to a certain extent and reduce the influence of multiplicative factors caused by changes in lighting conditions, also can distinguish the influence on the spectrum caused by the difference of the surface parameters.

5. Conclusions

This paper studies the pretreatment of soil hyperspectra and Na+ ion under different degrees of human activity stress, and carries out experiments such as soil sample collection, field spectrum measurements, spectral transformation and FOD. A FieldSpec®3Hi-Res spectrometer is used to measure the field ground hyperspectral of the soil, and the soil Na^+ ion content is determined by chemical detection methods. The Grünwald-Letnikov FOD is used to preprocess the soil original spectra and its transformed spectra (R, $\sqrt{R}$, 1/R, lgR, 1/lgR). The manuscript mainly focuses on the characteristics of the original hyperspectral reflectance curve of the soil pretreated by FOD, and the correlation coefficients between five transformed spectrum and soil Na^+ ion. In addition, the useful information hidden in the FOD of hyperspectra is examined in depth, the advantages of fractional-order and integer-order derivative to improve preprocessing are discussed, and the nonlinear characteristics and variation law of hyperspectral in the field of saline soil are revealed. The conclusions of the study could be summarized as follows: (1) With the increase of the order, the peak contour of the hyperspectral data is gradually changed, and the peak removal operation makes the original soil hyperspectral reflectivity curve pretreated by derivative gradually approach the rate of change of the slope of the curve. (2) The improvement of the correlation coefficient between the spectrum and Na^+ by the low-order derivative is relatively small, while the improvement of the high-order derivative is relatively large. (3) Although the change trend of the band numbers that passed the 0.01 level of significance test is different under different human disturbance areas, but in general, the hyperspectral bands that passed the 0.01 level test are mostly located at the high-order derivative. And there are many FOD bands in the original spectrum and its transformation that exceed the integer-order derivative. Therefore, this study collects the field VNIR-SWIR of soil samples in different human disturbance areas, preprocesses the VNIR-SWIR spectroscopy of the soil using FOD, and observes the details of the changes in the hyperspectral reflectance curve in different FOD. The feasibility of the application for FOD in the field hyperspectra under different degrees of human activity stress is verified.

Author Contributions: A.T. and J.Z. designed the research. A.T. and H.X. performed the experiment. C.F., B.T. and D.Z. participated in the data analysis. A.T. and B.T. revised the manuscript. All authors have read and agreed to the published version of the manuscript.

Funding: The authors would like to thank the National Natural Science Foundation of China under 41901065, 41671198, 42067029, 41761081, 41761041. Special Project of Teacher Education Research of Qujing Normal University under 2019JZ001. Key Project of Local Undergraduate Universities for Yunnan Provincial Department of Science and Technology under 2019FH001(-005).

Data Availability Statement: Not Applicable.

Acknowledgments: We would like to thank the Xinjiang Institute of Ecology and Geography for providing the chemical analysis soil salt content results.

Conflicts of Interest: The authors declare no conflict of interest.

References

1. Nurmemet, I.; Sagan, V.; Ding, J.L.; Halik, Ü.; Abliz, A.; Yakup, Z. A WFS-SVM Model for Soil Salinity Mapping in Keriya Oasis, Northwestern China Using Polarimetric Decomposition and Fully PolSAR Data. *Remote Sens.* **2018**, *10*, 598. [CrossRef]
2. Metternicht, G.I.; Zinck, J.A. Remote sensing of soil salinity: Potentials and constraints. *Remote Sens. Environ.* **2003**, *85*, 1–20. [CrossRef]
3. Farifteh, J.; Van der Meer, F.; Atzberger, C.; Carranza, E.J.M. Quantitative analysis of salt-affected soil reflectance spectra: A comparison of two adaptive methods (PLSR and ANN). *Remote Sens. Environ.* **2007**, *110*, 59–78. [CrossRef]
4. Peng, J.; Biswas, A.; Jiang, Q.S.; Zhao, R.Y.; Hu, J.; Hu, B.F.; Shi, Z. Estimating soil salinity from remote sensing and terrain data in southern Xinjiang Province, China. *Geoderma* **2019**, *337*, 1309–1319. [CrossRef]
5. Ma, L.; Ma, F.; Li, J.; Gu, Q.; Yang, S.; Wu, D.; Feng, J.; Ding, J. Characterizing and modeling regional-scale variations in soil salinity in the arid oasis of Tarim Basin, China. *Geoderma* **2017**, *305*, 1–11. [CrossRef]

6. Neha, J.; Matthias, B.; Andrea, E.; Rasmus, F.; Kenneth, G.; Patrick, H.; Martin, R.J.; Tobias, K.; Patrick, M.; Edward, T.A.M.; et al. A review of the application of optical and radar remote sensing data fusion to land use mapping and monitoring. *Remote Sens.* **2016**, *8*, 70.
7. Wang, H.; Chen, Y.; Zhang, Z.; Chen, H.; Chai, H. Quantitatively estimating main soil water-soluble salt ions content based on Visible-near infrared wavelength selected using GC, SR and VIP. *PeerJ* **2019**, *7*, e6310. [CrossRef] [PubMed]
8. Srivastava, R.; Sethi, M.; Yadav, R.K.; Bundela, D.S.; Barthwal, A.K. Visible-near infrared reflectance spectroscopy for rapid characterization of salt-affected soil in the Indo-Gangetic Plains of Haryana, India. *J. Indian Soc. Remote Sens.* **2017**, *45*, 307–315. [CrossRef]
9. Ferner, J.; Linstädter, A.; Südekum, K.H.; Linstaedter, A. Spectral indicators of forage quality in West Africa's tropical savannas. *Int. J. Appl. Earth Obs. Geoinf.* **2015**, *41*, 99–106. [CrossRef]
10. Shinya, T.; Kensuke, K.; Masayasu, M.; Yasunori, M.; Kazuaki, Y.; Tsuyoshi, A. Spectral index for quantifying leaf area index of winter wheat by field hyperspectral measurements: A case study in gifu prefecture, central Japan. *Remote Sens.* **2015**, *7*, 5329–5346.
11. Wang, J.; Shi, T.; Yu, D.; Teng, D.; Ge, X.; Zhang, Z.; Yang, X.; Wang, H.; Wu, G. Ensemble machine-learning-based framework for estimating total nitrogen concentration in water using drone-borne hyperspectral imagery of emergent plants: A case study in an arid oasis, NW China. *Environ. Pollut.* **2020**, *266*, 115412. [CrossRef]
12. Hong, Y.; Shen, R.; Cheng, H.; Chen, Y.; Zhang, Y.; Liu, Y.; Zhou, M.; Yu, L.; Liu, Y.; Liu, Y. Estimating lead and zinc concentrations in peri-urban agricultural soils through reflectance spectroscopy: Effects of fractional-order derivative and random forest. *Sci. Total. Environ.* **2019**, *651*, 1969–1982. [CrossRef] [PubMed]
13. Zhang, Z.; Ding, J.; Wang, J.; Ge, X. Prediction of soil organic matter in northwestern China using fractional-order derivative spectroscopy and modified normalized difference indices. *Catena* **2020**, *185*, 104257. [CrossRef]
14. Wang, X.; Zhang, F.; Kung, H.; Johnsone, V.C. New methods for improving the remote sensing estimation of soil organic matter content (SOMC) in the Ebinur Lake Wetland National Nature Reserve (ELWNNR) in northwest China. *Remote Sens. Environ.* **2018**, *218*, 104–118. [CrossRef]
15. Wang, J.; Tiyip, T.; Ding, J.; Zhang, D.; Liu, W.; Wang, F.; Tashpolat, N. Desert soil clay content estimation using reflectance spectroscopy preprocessed by fractional derivative. *PLoS ONE* **2017**, *12*, e0184836. [CrossRef]
16. Yang, X.; Yu, Y. Estimating soil salinity under various moisture conditions: An experimental study. *IEEE Trans. Geosci. Remote Sens.* **2017**, *55*, 2525–2533. [CrossRef]
17. Junhua, Z.; Pingping, J.; Yuan, S.; Keli, J. Prediction of salinity ion content in different soil layers based on hyperspectral data. *Trans. Chin. Soc. Agric. Eng.* **2019**, *35*, 106–115.
18. Zhang, J.; Sun, Y.; Jia, K.; Gao, X.; Zhang, X. Spectral Characteristics and Salinization Information Prediction of Different Soil Salt Crusts. *Trans. Chin. Soc. Agric. Mach.* **2018**, *49*, 325–333.
19. Ben-Dor, E.; Granot, A.; Notesco, G. A simple apparatus to measure soil spectral information in the field under stable conditions. *Geoderma* **2017**, *306*, 73–80. [CrossRef]
20. Francos, N.; Ben-Dor, E. A transfer function to predict soil surface reflectance from laboratory soil spectral libraries. *Geoderma* **2022**, *405*, 115432. [CrossRef]
21. Duan, P.; Xiong, H.; Li, R.; Zhang, L. A Quantitative Analysis of the Reflectance of the Saline Soil under different Disturbance Extent. *Spectrosc. Spectr. Anal.* **2017**, *37*, 571–576.
22. Dabiri, A.; Butcher, E.A. Stable fractional Chebyshev differentiation matrix for the numerical solution of multi-order fractional differential equations. *Nonlinear Dyn.* **2017**, *90*, 185–201. [CrossRef]
23. Guner, O.; Bekir, A. Exact solutions to the time-fractional differential equations via local fractional derivatives. *Waves Random Complex. Media* **2018**, *28*, 139–149. [CrossRef]
24. Atangana, A. Non validity of index law in fractional calculus: A fractional differential operator with Markovian and non-Markovian properties. *Phys. A Stat. Mech. Appl.* **2018**, *505*, 688–706. [CrossRef]
25. Zou, Y.; He, G. On the uniqueness of solutions for a class of fractional differential equations. *Appl. Math. Lett.* **2017**, *74*, 68–73. [CrossRef]
26. Kumar, D.; Seadawy, A.R.; Joardar, A.K. Modified Kudryashov method via new exact solutions for some conformable fractional differential equations arising in mathematical biology. *Chin. J. Phys.* **2018**, *56*, 75–85. [CrossRef]
27. Agarwal, R.P.; Baleanu, D.; Nieto, J.J.; Torres, D.F.M.; Zhou, T. A survey on fuzzy fractional differential and optimal control nonlocal evolution equations. *J. Comput. Appl. Math.* **2018**, *339*, 3–29. [CrossRef]
28. Baleanu, D.; Wu, G.C.; Bai, Y.R.; Chen, F.L. Stability analysis of Caputo–like discrete fractional systems. *Commun. Nonlinear Sci. Numer. Simul.* **2017**, *48*, 520–530. [CrossRef]
29. Farshad, M.B. A uniform LMI formulation for tuning PID, multi-term fractional-order PID, and Tilt-Integral-Derivative (TID) for integer and fractional-order processes. *ISA Trans.* **2017**, *68*, 99–108.
30. Tian, A.; Fu, C.; Xiong, H.; Yau, H.-T. Innovative Intelligent Methodology for the Classification of Soil Salinization Degree using a Fractional-Order Master-Slave Chaotic System. *Int. J. Bifurc. Chaos* **2019**, *29*, 1950026.
31. Khondoker, N.N.; Hamadjam, A.; Pushpendra, K. Forecasting of COVID-19 pandemic: From integer derivatives to fractional derivatives. *Chaos Solitons Fractals* **2020**, *141*, 110283.
32. Vasily, E.T.; Svetlana, S.T. Fractional and integer derivatives with continuously distributed lag. *Commun. Nonlinear Sci. Numer. Simul.* **2019**, *70*, 125–169.

33. Issam, A.I.; Marwan, A.; Mohammed, A.; Jaradat, I.; Noorani, M.S.M. Attractive new fractional-integer power series method for solving singularly perturbed differential equations involving mixed fractional and integer derivatives. *Results Phys.* **2021**, *20*, 103780.
34. Mihir, S.; John, P.H.; Fabio, S.; Bill, G. Implicit and fractional-derivative operators in infinite networks of integer-order components. *Chaos Solitons Fractals.* **2018**, *114*, 186–192.
35. Tian, A.; Fu, C.; Yao, H.-T.; Su, X.-Y.; Xiong, H. A New Methodology of Soil Salinization Degree Classification by Probability Neural Network Model based on Centroid of Fractional Lorenz Chaos Self-Synchronization Error Dynamics. *IEEE Trans. Geosci. Remote Sens.* **2020**, *58*, 799–810. [CrossRef]
36. Debdoot, S.; Mohan, B.M. A simple approach to mathematical modelling of integer order and fractional order fuzzy PID controllers using one-dimensional input space and their experimental realization. *J. Frankl. Inst.* **2021**, *358*, 3726–3756.